**@**⊕\$≘



#### **ACCEPTED MANUSCRIPT**

## Calibrating the global network of gravitational wave observatories via laser power calibration at NIST and PTB

To cite this article before publication: Dripta Bhattacharjee et al 2024 Metrologia in press https://doi.org/10.1088/1681-7575/ad615f

### Manuscript version: Accepted Manuscript

Accepted Manuscript is "the version of the article accepted for publication including all changes made as a result of the peer review process, and which may also include the addition to the article by IOP Publishing of a header, an article ID, a cover sheet and/or an 'Accepted Manuscript' watermark, but excluding any other editing, typesetting or other changes made by IOP Publishing and/or its licensors"

This Accepted Manuscript is © 2024 BIPM & IOP Publishing Ltd.

During the embargo period (the 12 month period from the publication of the Version of Record of this article), the Accepted Manuscript is fully protected by copyright and cannot be reused or reposted elsewhere.

As the Version of Record of this article is going to be / has been published on a subscription basis, this Accepted Manuscript will be available for reuse under a CC BY-NC-ND 3.0 licence after the 12 month embargo period.

After the embargo period, everyone is permitted to use copy and redistribute this article for non-commercial purposes only, provided that they adhere to all the terms of the licence <a href="https://creativecommons.org/licences/by-nc-nd/3.0">https://creativecommons.org/licences/by-nc-nd/3.0</a>

Although reasonable endeavours have been taken to obtain all necessary permissions from third parties to include their copyrighted content within this article, their full citation and copyright line may not be present in this Accepted Manuscript version. Before using any content from this article, please refer to the Version of Record on IOPscience once published for full citation and copyright details, as permissions may be required. All third party content is fully copyright protected, unless specifically stated otherwise in the figure caption in the Version of Record.

View the article online for updates and enhancements.

# Calibrating the global network of gravitational wave observatories via laser power calibration at NIST and PTB

- D. Bhattacharjee<sup>1,2</sup>, R. L. Savage<sup>3</sup>, R. Bajpai<sup>4</sup>,
- J. Betzwieser<sup>5</sup>, V. Bossilkov<sup>5</sup>, D. Chen<sup>6</sup>, C. Grimaud<sup>8</sup>,
- S. Hido<sup>7</sup>, S. Karki<sup>2</sup>, S. Kück<sup>9</sup>, P. Lagabbe<sup>8</sup>, H. Lecher<sup>9</sup>,
- J. Lehman<sup>10</sup>, F. Llamas<sup>11</sup>, M. López<sup>9</sup>, L. Rolland<sup>8</sup>,
- A. Sanchez<sup>3</sup>, M. Spidell<sup>10</sup>, and M. Stephens<sup>10</sup>

Particules - IN2P3, F-74000 Annecy, France

E-mail: dripta.bhattacharjee@ligo.org, rsavage@caltech.edu

**Abstract.** Current gravitational wave observatories rely on photon calibrators that use laser radiation pressure to generate displacement fiducials used to calibrate detector output signals. Reducing calibration uncertainty enables optimal extraction of astrophysical information such as source distance and sky position from detected signals. For the ongoing O4 observing run that started on May 24, 2023, the global gravitational wave detector network is employing a new calibration scheme with transfer standards calibrated at both the National Institute of Standards and Technology (NIST) and the Physikalisch-Technische Bundesanstalt (PTB). These transfer standards will circulate between the observatories and the metrology institutes to provide laser power calibration traceable to the International System of Units (SI) and enable assessment and reduction of relative calibration errors for the observatory network. The Laser Interferometer Gravitational-Wave Observatory (LIGO) project and the Virgo project are currently participating in the new calibration scheme. The Large-scale Cryogenic Gravitational-wave Telescope project (KAGRA) is expected to join in 2024, with the LIGO Aundha Observatory (LAO) in India joining later. Before implementing this new scheme, a NIST-PTB bilateral comparison was conducted. It validated the scale representation by both laboratories, with a degree of equivalence of -0.2% and an associated expanded uncertainty of 0.32% (k=2) which is significantly lower than previous studies. We describe the transfer of power sensor calibration, including detailed uncertainty estimates, from the transfer standards calibrated by

<sup>&</sup>lt;sup>1</sup>Kenyon College, Gambier, USA

<sup>&</sup>lt;sup>2</sup>Missouri University of Science and Technology, Rolla, USA

<sup>&</sup>lt;sup>3</sup>LIGO Hanford Observatory, Richland, USA

<sup>&</sup>lt;sup>4</sup>National Astronomical Observatory of Japan, Mitaka, Japan

<sup>&</sup>lt;sup>5</sup>LIGO Livingston Observatory, Livingston, USA

<sup>&</sup>lt;sup>6</sup>National Astronomical Observatory of Japan, Hida, Japan

<sup>&</sup>lt;sup>7</sup>Institute for Cosmic Ray Research, Kashiwa, Japan

<sup>&</sup>lt;sup>8</sup>Université Savoie Mont Blanc, CNRS, Laboratoire d'Annecy de Physique des

<sup>&</sup>lt;sup>9</sup>Physikalisch-Technische Bundesanstalt, Braunschweig, Germany

<sup>&</sup>lt;sup>10</sup>National Institute of Standards and Technology, Boulder, USA

<sup>&</sup>lt;sup>11</sup>University of Texas Rio Grande Valley, Brownsville, USA

NIST and PTB to the sensors operating continuously at the interferometer end stations. Finally, we discuss the ongoing calibration of Pcal-induced displacement fiducials for the O4 observing run. Achieved combined standard uncertainty levels as low as  $0.3\,\%$  facilitate calibrating the interferometer output signals with sub-percent accuracy.

Submitted to: Metrologia



### 1. Introduction

Gravitational wave (GW) observatories use kilometer-scale variants of Michelson interferometers with modifications such as optical resonators that increase their sensitivity to differential arm length variations to the  $10^{-20}$  m level. Since the first direct detection of GWs from a coalescing binary black hole system in 2015 [1], the network of GW observatories has detected nearly one hundred GW signals from coalescing compact binary sources [2], yielding insight into source properties [3, 4], formation processes [5, 6, 7], populations [8], and cosmological parameters [9, 10, 11]. Eventually, for optimal extraction of this astrophysical information calibration of the interferometer output signals with sub-percent accuracy will be required [12, 13].

Calibrating the data from GW detectors involves converting the interferometer output signals into meters of differential arm (DARM) length variation. Maintaining suspended interferometer optics in their optimal positions and orientations requires multiple feedback control loops, including the so-called DARM loop that suppresses variations in the differential arm length degree of freedom. Thus, reconstructing the differential length variations induced by GWs requires accurately characterizing the DARM control loop. This is achieved using calibrated periodic fiducial displacements of the mirrors or end test masses (ETMs) located at the ends of the perpendicular arms of the interferometer. These periodic displacements are induced by systems referred to as photon calibrators (Pcals) that use the radiation pressure from power-modulated auxiliary laser beams reflecting from the mirror surfaces to periodically displace the ETMs [14]. Periodically modulating the Pcal laser by 30 mW at 300 Hz modulates the position of the 40 kg ETM by about  $10^{-18}$  m. The amplitude of the Pcal-induced length variations is proportional to the amplitude of the modulated Pcal laser power. Thus, the accuracy of the periodic fiducial displacements is directly dependent on the accuracy of the calibration of the Pcal laser power sensors.

To date, the calibration of Pcal laser power sensor responsivity, in volts per watt, has been provided by the national metrology institute (NMI) in the USA, NIST, in Boulder, Colorado. The methods developed and employed to transfer the NIST calibration of Pcal power sensors to Pcal power sensors continuously operating at the observatory end stations enabled Pcal-induced fiducial displacements with sub-percent accuracy for previous observing runs [15, 16].

For the ongoing O4 observing run, the two LIGO detectors [17], at the LIGO Hanford Observatory (LHO) and the LIGO Livingston Observatory (LLO), the Virgo detector [18, 19], and the KAGRA detector [20] are either already participating or planning to join in the near future. To further reduce uncertainties, to increase confidence in our calibration accuracy, and to reduce relative calibration errors between observatories in the GW network, a new calibration scheme with two transfer standards traveling around a loop that includes both NIST and PTB and the participating GW observatories has been developed for the O4 observing run. Before implementing the new global calibration scheme, a second NIST-PTB bilateral comparison with Pcal-

style laser power sensors was conducted. The first NIST-PTB bilateral comparison was carried out in 2020.

The results of the new comparison are presented in section 2 together with a description of the new global calibration scheme. In section 3 we present the formalism for the test mass displacement induced by power-modulated Pcal beams, including the impact of unintended induced rotation of the ETM. In section 4 we describe the process of propagating Pcal power sensor calibration at NIST and PTB to the Pcal sensors operating at the interferometer end stations, including uncertainty estimates. In section 5 we describe the calibration of the Pcal-induced displacement fiducials and the reduction in uncertainty achieved by using the interferometer signals to make low-uncertainty measurements of the ratio of the Pcal calibrations at the two end stations of the interferometer. Conclusions are presented in section 6.

### 2. New global calibration scheme and recent NIST-PTB bilateral comparison

The GW community is striving to achieve interferometer displacement calibration with uncertainties below 1% across the sensitive detection frequency band from approximately 10-20 Hz to 2 kHz [21, 22, 23]. Achieving this level of calibration accuracy requires displacement fiducials with sub-percent accuracy. All of the detectors in the GW network use Pcal systems to generate these calibrated fiducial displacements [24, 25, 26]. Historically, Pcal laser power sensor calibration has been achieved using Pcal transfer standards calibrated by NIST, eventually achieving combined standard displacement uncertainty as small as 0.41% at LHO during the O3 observing run in 2019-20 [16]. Calibrated Pcal power sensors based on the NIST calibrations were also used to calibrate Virgo and KAGRA Pcal power standards during the O3 observing run. This enabled identifying and eliminating a significant relative calibration discrepancy between the LIGO and Virgo detectors [27]. However, coupling the Pcal sensors for all detectors to a single standard calibrated at one NMI risks introducing a systematic error for the whole GW network.

To increase confidence in calibration accuracy a first bilateral comparison between NIST and PTB using a single LIGO Pcal power standard at 100 mW and 300 mW power levels and at the 1047 nm Pcal laser wavelength used by all detectors was conducted in 2020. The results are reported in [28] and summarized in table 1. For that comparison the NIST and PTB calibrations had relative combined standard uncertainties of 0.42% and 0.10%, respectively. The composite bilateral degree of equivalence (DoE) [29], of -0.15% with expanded uncertainty of 0.87% (k=2) indicated that the scale representations realized by both NMIs were consistent with each other [28].

Pcal power standards similar to those used for this comparison and to those used by all observatories are shown in figure 1. They consist of 10-cm-diameter integrating spheres with diffuse-scattering Spectralon<sup>®</sup> interior shells (Labsphere model 3P-LPM-040-SL), unbiased InGaAs photodetectors, and custom-built, integrated transimpedance

**Table 1.** Key results - consensus responsivity (CR), degree of equivalence (DoE), relative combined standard uncertainties  $(u_{c,rel})$ , and expanded relative uncertainty  $(U_{rel})$  - for NIST-PTB bilateral comparisons using Pcal-style power sensors: WSS in 2020 and O4 transfer standards TSA and TSB in 2023. All measurements were made with approximately 300 mW of 1047 nm laser radiation.

Year	Sensor	$\mathrm{CR}/(\mathrm{V}/\mathrm{W})$	$u_{c,rel}/\%$	$\mathrm{DoE}/\%$	$U_{rel}/\%~(k{=}2)$
2020	WSS	-8.189	0.10	-0.15	0.87
2023	TSA TSB	-4.3594 -4.2743	0.08 0.08	-0.20	0.32



**Figure 1.** Two upgraded Pcal laser power sensors, similar to those used for transfer standards, TSA and TSB. The red-anodized components are spacers with an internal aperture that were added after the O3 observing run to reduce the temperature dependence of the responsivity.

amplifiers. These sensors were upgraded after the first bilateral comparison, between the O3 and O4 observing runs, to add spacers with internal apertures between the photodetectors and the integrating spheres and to simplify the transimpedance amplifier electronics. Temperature sensors (Analog Devices AD590) were also added to the circuit boards. The spacers reduced the temperature dependence of the responsivity by about a factor of four to 0.02 - 0.03% per kelvin.

For the O4 observing run we developed a new global calibration scheme [30] that is shown schematically in figure 2. Two transfer standards, referred to as TSA and TSB, of the same design as those shown in figure 1 circulate around a loop that

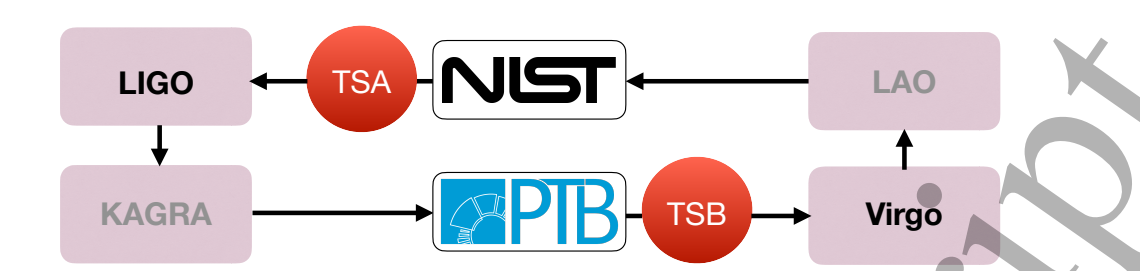


**Figure 2.** Schematic diagram of global calibration scheme with transfer standards TSA and TSB traveling around a loop between LIGO, PTB, Virgo, and NIST once per year. KAGRA is expected to join the scheme in 2024 with LAO joining later.

includes participating observatories, NIST, and PTB, once per year. TSA and TSB are delayed by six months with respect to each other such that each observatory receives a recently-calibrated transfer standard every six months and each transfer standard is calibrated twice per year, once at PTB and once at NIST. Currently only Virgo and LIGO are participating in this scheme, but KAGRA is planning to join in 2024 and LAO, under construction in Maharashtra, India, will likely join in the future. This scheme is designed to reduce relative uncertainties between participating observatories, continue the NIST-PTB bilateral comparison, and identify potential changes in transfer standard responsivities that might occur during shipment or during measurements at the observatories or NMIs.

In 2023, before the beginning of the O4 observing run and before implementing the global calibration scheme, a second NIST-PTB bilateral comparison was carried out. For this comparison, transfer standards, TSA and TSB, were used. Also, a new-generation primary calibration standard ‡ at NIST, referred to as a PARRoT detector [31], was used for these calibrations. The reference standard detector used by PTB is a cavity-based thermal detector with traceability to a cryogenic radiometer [32, 33] primary standard established via a Si-trap detector transfer standard [34]. The relative combined standard calibration uncertainty of the PARRoT detector is 0.07%, significantly smaller than NIST's previous calibrations (0.31 % - 0.42 %), and comparable to the PTB calibration uncertainty [28]. For the more recent bilateral comparison TSA and TSB were first sent for calibration to NIST, then to PTB, and finally back to NIST. The measured responsivities of the transfer standards,  $\rho_T$ , normalized to their respective consensus responsivity (CR) for this second bilateral comparison are shown in figure 3. The key results are included in table 1. The DoE between the NIST and PTB results was calculated using the formalism outlined in Appendix B of [29] as for the previous comparison [28]. It is -0.20 % with expanded relative uncertainty of 0.32 % (k=2). This

‡ By primary calibration standard, we mean a calibration standard that is directly traceable to SI without using an additional reference standard. This is typically accomplished by electrical substitution methods relying on the ampere and the ohm.

uncertainty is more than a factor of two smaller than for the first bilateral comparison, mostly due to the new PARRoT primary standard at NIST. The observed DoE is still less than its expanded relative uncertainty, i.e. within the 95% confidence interval.

After completing this comparison, TSA was delivered to LIGO and TSB to Virgo where they were used to calibrate the *gold standard* power sensors as described in section 4. Now, in February 2024, they are at PTB and NIST for calibration, continuing with the O4 global calibration scheme.

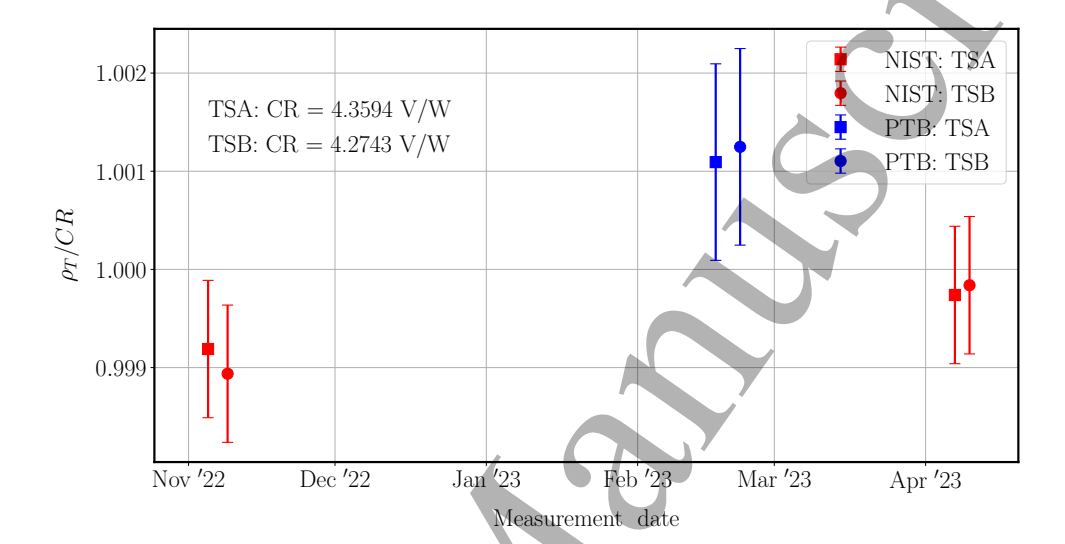
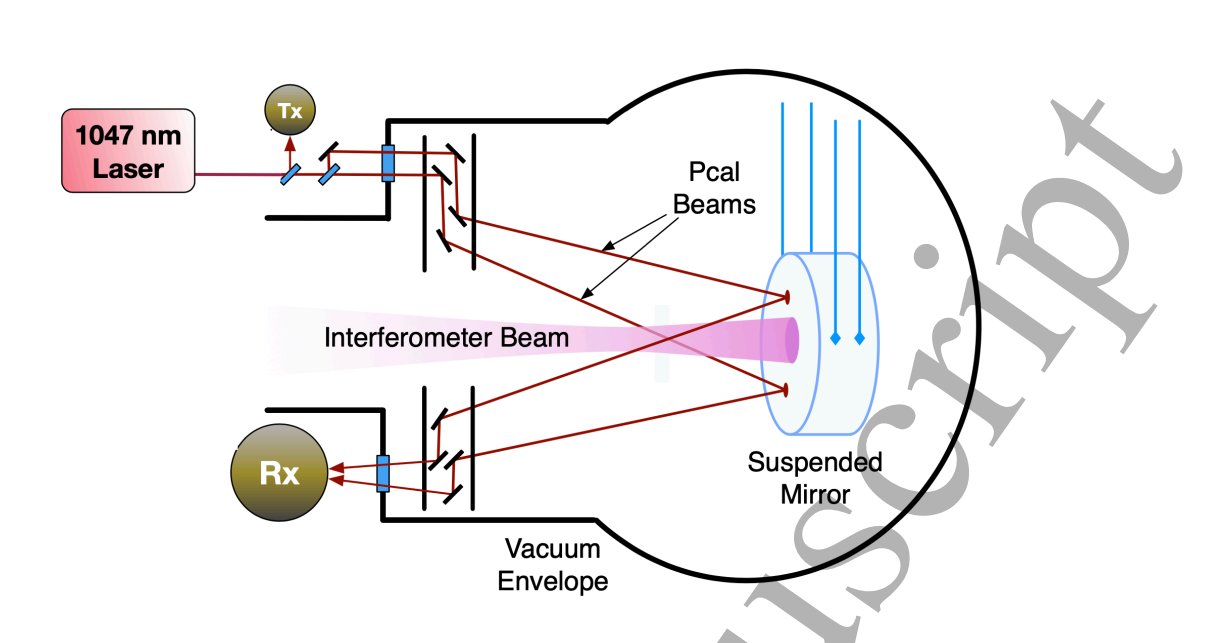


Figure 3. Responsivities of transfer standards TSA and TSB measured at NIST and PTB, each normalized to the respective consensus responsivity CR. All data are propagated to 300.15 K using measured responsivity temperature coefficients. This is a typical temperature reported by the on-board temperature sensor that operates at about 6 K above ambient temperature. The error bars represent the relative standard uncertainties of the measurements.

### 3. Fiducial displacements induced by photon calibrators

A schematic diagram of a typical Pcal system is shown in figure 4. The output of an auxiliary laser is divided in a transmitter (Tx) module into two beams that impinge on a suspended mirror at locations equally spaced and diametrically opposed about the center of mass of the mirror. This two-beam configuration is designed to minimize elastic deformation of the surface of the mirror in the region sensed by the interferometer beam, nominally the center of the surface [35]. They are located close to the nodal circle of the natural drumhead vibrational mode of the mirror to minimize sensing of induced bulk elastic deformation of the ETM by the interferometer [24]. Both the LIGO and the KAGRA interferometers use two beams [15, 36]; the Virgo interferometer currently uses one beam centered on the ETM surface and compensates for the impact of local deformation of the ETM surface by modeling [25, 27]. The laser light reflected from the



**Figure 4.** Schematic diagram of a typical two-beam Pcal system. The power modulated Pcal laser is divided in a transmitter (Tx) module and directed toward the mirror surface. The reflected light is directed to a Pcal power sensor in the receiver (Rx) module. The mirror diameter is 32 cm and the optical path length between the Tx and Rx power sensors is about 12 m.

ETM is directed toward a receiver (Rx) module and captured by the Pcal Rx power sensor. A Pcal Tx power sensor captures a small fraction of the input Pcal light and is used for calibrating the optical efficiency which must be taken into account to estimate the laser power reflecting from the ETM surface. It is also used for measurements made to calibrate the Rx sensor.

The periodic force exerted by power-modulated Pcal laser beam(s) reflecting from the surface of a suspended ETM is given by

$$F(\omega) = \frac{2\cos\theta}{c}P(\omega). \tag{1}$$

Here  $\theta$  is the angle of incidence of the Pcal beam(s) on the ETM surface, c is the speed of light,  $P(\omega)$  is the amplitude of the modulated laser power reflected from the ETM surface, and  $\omega = 2\pi f$  is the angular frequency of the power modulation.

The Pcal forces can also induce unintended and unwanted rotation of the ETM [24] due to either power imbalance between the two Pcal beams or due to beam position offsets from their ideal locations. If the interferometer beam is offset from its nominal centered location, rotations of the ETM will be sensed as length variations by the interferometer, resulting in mis-calibration of Pcal-induced displacement fiducials when assuming simple pendulum motion of the ETM.

The Pcal-induced ETM displacement sensed by the interferometer is given by

$$x(\omega) = -\frac{2\cos\theta}{Mc\omega^2}P(\omega)\left[1 + \frac{M}{I}(\vec{a}\cdot\vec{b})\right],\tag{2}$$

where M is the mass of the suspended optic, I is the moment of inertia for rotation of the ETM about an axis through its center of mass and parallel to the face of the optic,  $\vec{a}$  is the displacement vector from the center of the surface of the optic to the position of the center of force of the Pcal beams and  $\vec{b}$  the displacement vector for the interferometer beam. The first term within the square brackets (unity) is for the longitudinal displacement of the ETM and the second term is for the sensed longitudinal displacement due to unintended rotation of the ETM. The negative sign indicates that the ETM motion is  $180^{\circ}$  out of phase with the exerted force for modulation frequencies well above the pendulum and rotation resonance frequencies, both near 1 Hz.

In practice, although the magnitude and direction of  $\vec{b}$  can be estimated from angle-to-length coupling measurements performed with the interferometer and the ETM suspension actuators, neither the magnitude nor the direction of  $\vec{a}$  are known. Only its maximum expected magnitude can be estimated, after having carefully located the Pcal beams on the ETM surface when the vacuum system was vented and subsequently monitoring the positions of the reflected Pcal beams at the input aperture of the Rx sensor [15]. Therefore the second term in the square brackets is treated as an uncertainty in the displacement amplitude introduced by potential unintended rotation of the ETM. Thus accurate calibration of the Pcal laser power sensors that receive the beams reflected from the ETM, compensated for optical losses after reflection, is the primary challenge for estimating Pcal induced displacement amplitudes.

### 4. Propagation of calibration from transfer standards to Pcal power sensors at interferometer end stations

The procedure for propagating the calibration of the responsivity of the transfer standards to the Pcal Rx sensors operating at the interferometer end stations is shown schematically in figure 5. Responsivity ratio measurements performed in a dedicated laboratory at the observatory are used to propagate the calibration from a transfer standard (TS) that was calibrated by either NIST or PTB to a gold standard (GS) that is maintained in the laboratory. The measurements are made using a 1047 nm laser that is power-stabilized with its output divided into two beams of roughly equal powers [15] of close to 300 mW. The two power standards are mounted on actuated slides that enable swapping the positions of the sensors between the two beams. Time series of the power sensor outputs are recorded simultaneously (within 100 ms), minimizing the impact of laser power variations on the ratio of the two signals. A second set of time series are recorded with the sensor position swapped. The square root of the product of the ratios of each pair of time series gives the GS/TS responsivity ratio,  $\alpha_{GT}$ , minimizing the impact of potential variations in the beamsplitter ratio during the measurements. One set of measurements requires about 20 s: 5 s of data, swapping positions, 5 s of data, swapping positions. The measurements are repeated approximately 100-300 times, so the whole process takes about 20 minutes to one hour. Multiplying this responsivity ratio by the responsivity of the TS provides responsivity of the GS, an SI-traceable

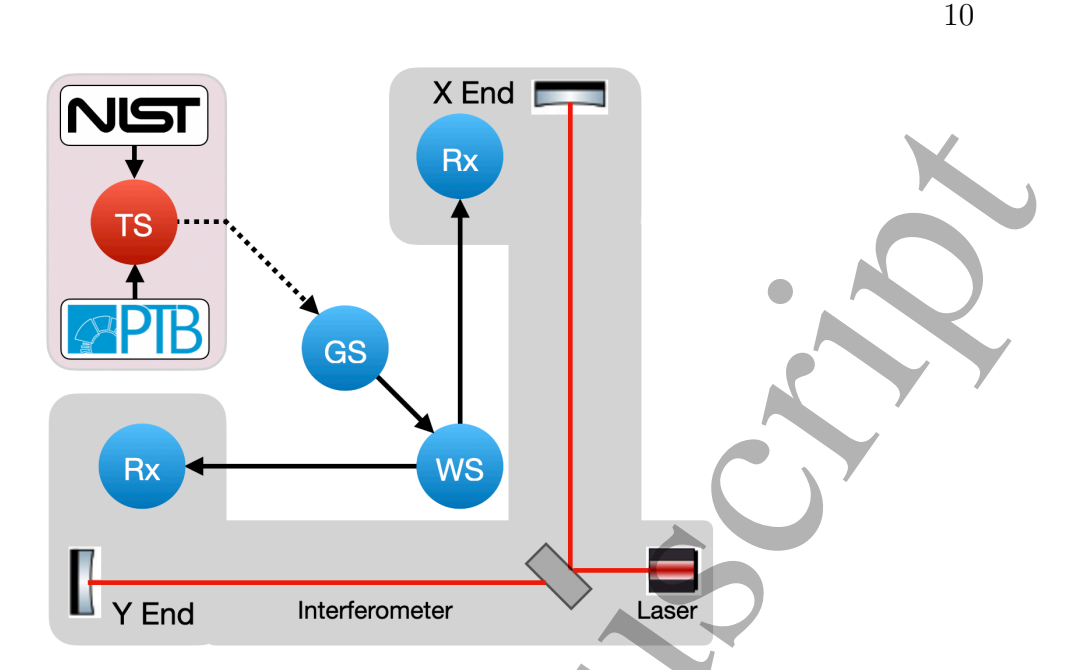


**Figure 5.** Schematic diagram of the steps involved in transferring calibration from a transfer standard (TS) to Rx sensors at the interferometer end stations via a *gold standard* (GS) and a *working standard* (WS).

representation of scale for optical radiant flux (i.e. optical power).

A similar procedure is used to transfer the GS responsivity to an identical power sensor, a working standard (WS), that is taken to the observatory end stations to calibrate the Pcal Rx sensors in the receiver modules. Calibration of the Rx sensors involves placing the WS inside the Tx module, intercepting one beam at a time, and recording time series of both the WS and Tx power sensor outputs. The working standard is then moved to the Rx module, replacing the Rx sensor, and time series of the WS and Tx sensors are again recorded, one beam at a time. Finally the Rx sensor is returned to the Rx module and Rx and Tx sensor time series are simultaneously recorded, one beam at a time. Detector backgrounds are measured by closing the laser shutter in the Tx module. A calibrated voltage source is used to calibrate the signal chain, primarily the conversion of the analog to digital converter (ADC) in counts per volt, of the data acquisition system [37] and to verify the calibration of a dedicated digital voltmeter in the responsivity ratio measurement laboratory. The temperature sensor on the WS transimpedance amplifier board is used to correct for temperature differences between the end station and the measurement laboratory.

The analysis of these measured time series yields the responsivity of the Rx sensor and the optical losses on the beam paths between the Tx and Rx sensors due to relay mirrors and the vacuum windows. Measurements made inside the vacuum envelope when the system is vented enable apportioning the optical losses between the beam paths on the ETM incidence and reflection sides. We assume that the ratio remains constant though the overall optical losses might vary slightly. Thus we are able to calibrate the Rx sensor in terms of the power reflecting from the ETM, rather than

the power incident on the Rx sensor, which is the relevant quantity for Pcal-induced displacement of the ETM. This is discussed in more detail in section 5.

The top panels in figure 6 show a typical suite of WS/GS responsivity ratio,  $\alpha_{WG}$ , measurements made in the Pcal laboratory at LHO [16] and at the Laboratoire d'Annecy de Physique des Particules (LAPP) in Annecy, France [38]. The means and relative standard deviations of the data are shown in the legends. The ranges of the vertical scales are the same for the LHO and LAPP plots to highlight that the variations in the LAPP data are much smaller than those in the LHO data, though they are similar to previous measurements made during the O3 observing run at LHO [16]. This seems to

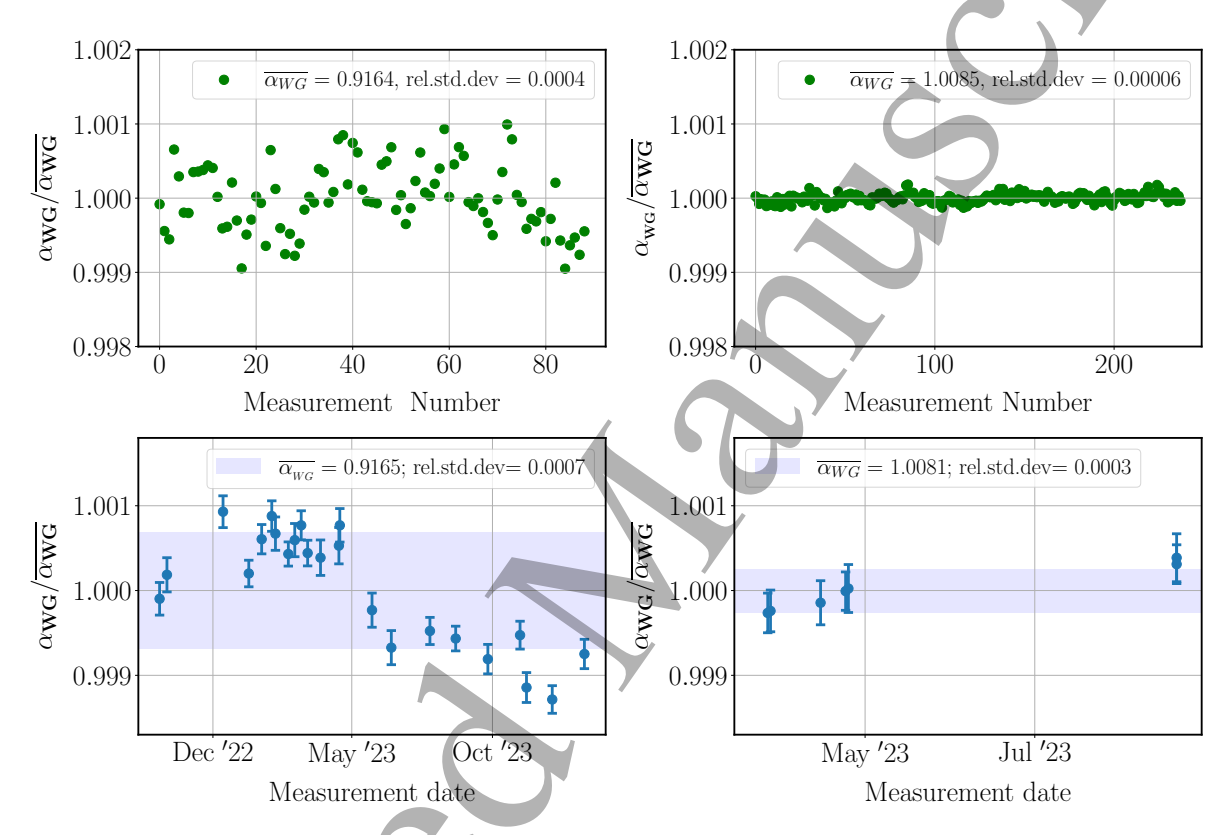


**Figure 6.** Top: A typical suite of measured  $\alpha_{WG}$  values in (V/W)/(V/W) at LHO (Left) and LAPP (Right). Bottom:  $\alpha_{WG}$  values measured at LHO (Left) and LAPP (Right) between Oct. 2022 and Jan. 2024. The error bars represent the relative standard uncertainties. They have been magnified for visibility: by a factor of 5 for the LHO data and by a factor of 50 for the LAPP data. The colored bands represent the relative standard deviations about the normalized weighted means.

indicate an issue with the LHO measurement setup and underscores one advantage of comparing similar measurements made in different facilities. The bottom panels in the figure 6 show  $\alpha_{WG}$  measured over spans that include the beginning of the O4 observing run, each corrected to the reference temperature of 300.15 K. Again, the vertical axis spans are the same. The error bars, relative standard uncertainties, have been magnified to increase visibility: by a factor of 5 for the LIGO data and by a factor of 50 for the LAPP data. The variations in the data are larger than what would be expected based

on standard uncertainties of the repeated measurements, indicating that there is a time-varying factor in the measurement process and the associated uncertainty has not been identified and taken into account. The LHO data also show an unexpected decrease of 0.10 - 0.15% in the ratio after May 2023. The cause of this decrease has not yet been identified. The colored bands indicate the relative standard deviation of the combined data set for both end stations, each normalized to their respective mean values. They are used to estimate the uncertainty in a single measurement of the WS/GS responsivity ratio. Because the TS sensors are identical by design and the measurement of  $\alpha_{GT}$  follows the same procedure as the  $\alpha_{WG}$  measurements, we use these uncertainty estimates for  $\alpha_{GT}$  as well.

Both LHO and LLO measure Rx/WS responsivity ratios,  $\alpha_{RW}$ , using the procedures described earlier in this section. As an example, the LHO ratios measured at both LHC

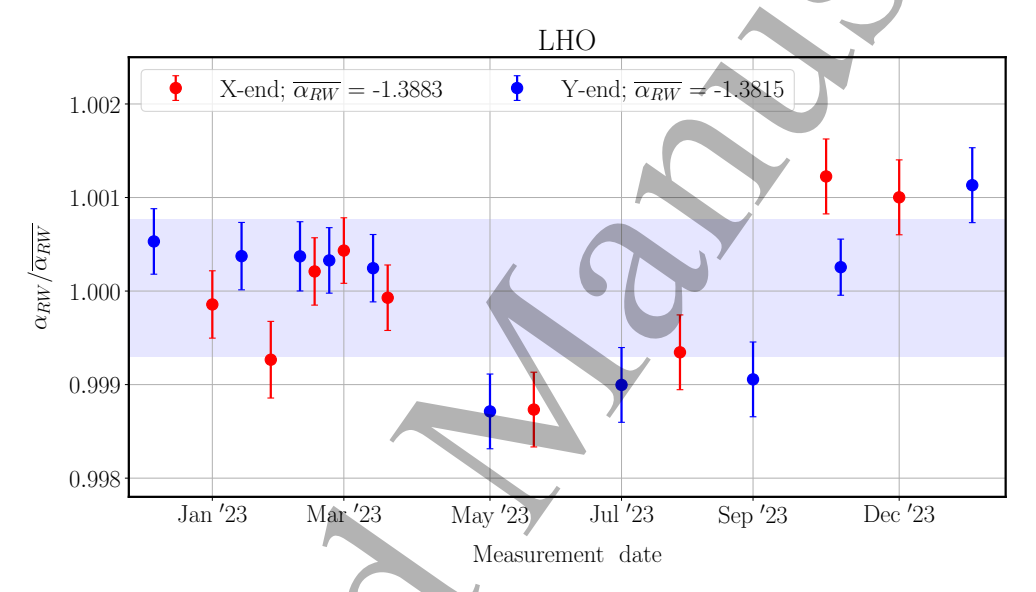


Figure 7. Measured  $\alpha_{RW}$  values in (count/watt)/(count/watt) for the LHO Rx sensors at the end stations. The data for each end station are normalized to their respective mean values. The error bars are combined standard uncertainties derived from the various time series involved in the end station measurements. The colored band denotes the relative standard deviation of all of the measurements normalized to their respective means.

measured Rx/WS responsivity ratios dip by  $\sim 0.15\%$  between April and Nov. 2023. The source of these unexpected dips is unknown and actively being investigated. It appears to be associated with outside temperature variations. As in figure 6, the colored band represents the relative standard deviation about the relative mean for all of the measurements and is used to estimate the uncertainty in a single measurement of  $\alpha_{RW}$ .

At Virgo,  $\alpha_{RW}$  was measured at both end stations in Nov. 2022 and again in June 2023. The measured ratio increased by about 0.2 % at the north end station and decreased by about 0.2 % at the west end station. Small alignment changes in the Pcal

modules were made in June 2023, but they were not expected to impact the responsivity of the Rx sensors.

The relative standard uncertainties in the Rx sensor responsivities and their contributing parameters for the LHO and Virgo end stations are shown in table 2. The uncertainties in the contributing factors are estimated following the formalism

**Table 2.** Relative standard uncertainties (%) for the measured responsivities of the LHO and Virgo Pcal Rx sensors at the end stations and their contributing uncertainties. Asterisks denote parameters that are NOT common to both end stations.

Parameter	Units	LHO		Virgo	Type		
or Source		X-end	Y-end				
*Rx resp., $\rho_{Rx}$	count/W	0.14	0.17	0.15	$u_{c,rel}$		
Contributing Uncertainties							
TS resp., $\rho_T$	V/W	0.08	0.08	0.08	$u_{c,rel}$		
Resp. ratio, $\alpha_{GT}$	(V/W)/(V/W)	0.07	0.07	0.03	$u_{rel,\mathrm{Type}\mathrm{B}}$		
Resp. ratio, $\alpha_{WG}$	(V/W)/(V/W)	0.07	0.07	0.03	$u_{rel,\mathrm{Type}\mathrm{B}}$		
*Resp. ratio, $\alpha_{RW}$	(count/W)/(count/W)	0.07	0.07	0.10	$u_{rel,\mathrm{Type}\mathrm{B}}$		
$\rho_{WS}$ temp. dep.	(V/W)/K	0.02	0.02	0.04	$u_{rel,\mathrm{Type}\mathrm{B}}$		
*ADC conversion	count/V	0.004	0.007	0.05	$u_{rel,\mathrm{Type}\mathrm{B}}$		

described in [39] with the type of uncertainty estimate noted in the table. For the responsivity ratios, the Type B uncertainties are derived from the colored bands in figure 6 and figure 7, as described above; approximately two thirds of the data are within the colored bands. The combined standard uncertainties for the TSA and TSB consensus responsivities,  $\rho_T$ , from the recent NIST-PTB bilateral comparison were calculated using the formalism detailed in [29].

### 5. LHO and Virgo Pcal-induced displacement fiducials and estimated uncertainties for the O4 observing run

The Rx sensors at the end stations are located outside the vacuum envelope as shown in figure 4 and receive the Pcal beams reflected from the ETM after reflection from relay mirrors and transmission through the vacuum window. The optical losses between the ETM and the Rx sensor must be taken into account to estimate the Pcal laser power reflecting from the ETM, as stated in section 4. As mentioned earlier, in-chamber measurements made in LIGO when the vacuum chamber is vented allow apportioning the total optical loss between the input and output sides of the ETM with the assumption that their ratio remains constant and any measured increase or decrease in overall loss can be similarly apportioned. As for LIGO, the Virgo Rx sensors are placed outside vacuum and their calibration must be compensated for the optical losses of the vacuum windows and one relay mirror in the in-air receiver module. Unlike LIGO, no relay optics

are present in the vacuum envelope; the beam reflected by the ETM goes directly out through the window. However, in-situ measurement at the end station of the optical losses were not feasible because of the lack of space to accommodate the WS in the transmitter module and in-chamber measurements have not been made. Hence, the optical losses were estimated by characterizing the losses (predominantly reflection) of the relay mirrors before they were installed at the end stations and of a spare vacuum window assumed to be a representative sample for the installed windows.

The induced periodic displacement in (2) can be rewritten in terms of the digitized output of the Rx sensor recorded by the data acquisition system at the end station as

$$x(\omega) \simeq -\frac{2\cos\theta}{M\,c\,\omega^2} \frac{d_R(\omega)}{\eta_R\,\rho_R} = -\frac{X}{\omega^2} \,d_R(\omega)\,,$$
 (3)

where  $d_R(\omega)$  is the digital output of the sensor in counts,  $\eta_R$  is the optical efficiency correction factor for the output side and  $\rho_R$  is the responsivity of the Rx sensor discussed in section 4. The frequency independent displacement calibration factor, X, is defined as

$$X = \frac{2\cos\theta}{Mc} \frac{1}{\eta_R \rho_R}.$$
 (4)

Uncertainty in this displacement calibration factor includes contributions from uncertainties in the angle of incidence, the mass of the ETM, and the optical efficiency. Because the magnitude and direction of any unintended misplacement of the Pcal beams on the ETM surface are unknown (see section 3), the rotational term in (2) is treated as a Type B uncertainty contribution for X and hence doesn't appear in (3). For Virgo, where single-beam Pcal systems are used, there is an additional contribution from the deformation modeling required to compensate for ETM deformations sensed by the interferometer. The estimated uncertainty in this contribution is valid up to  $\sim 1 \text{ kHz}$ , but increases significantly at higher frequencies. These contributions are listed in table 3.

GW interferometers are optimized to sense differential length variations, i.e. variations in the difference between the lengths of the two arms of the interferometer. However, except for the sign of the relative displacement, they are exquisitely insensitive to which arm length is varying. For the LIGO interferometers, calculations and modeling indicate that the deviations from this ideal due to observed variations in optical parameters are well below the 0.0001% level [40]. Thus, the interferometer signals enable very precise measurement of the ratio of the calibrations of the Rx sensor outputs at the two end stations, in terms of the power reflecting from the ETMs.

For the O4 observing run at LHO, the X/Y Pcal calibration comparison has been calculated continuously in the on-line front-end code of the control and data acquisition system. Following the method detailed in [16], ETM displacements with signal-to-noise (SNR) ratios of  $\sim 1000$  were induced by the Pcal systems at 283.91 Hz (X-end) and 284.01 Hz (Y-end). These induced periodic displacements appear in the interferometer output signal and in the Rx power sensor signals. The X/Y ratio of the amplitudes of peaks in spectra of the calibrated X-end and Y-end Pcal Rx sensor signals, divided

**Table 3.** Relative standard uncertainties (%) in displacement factors and contributing parameters for the LHO and Virgo end station Rx sensors. All parameters are NOT common to both end stations.

Parameter	Units	LHO		Virgo	Type
or Source		X-End	Y-End		
$X_{\scriptscriptstyle X}^c$ and $X_{\scriptscriptstyle Y}^c$	$\rm zm/(s^2count)$	0.29	0.29	_	$u_{c,rel}$
Contributing U					
$C_{\scriptscriptstyle X}$ and $C_{\scriptscriptstyle Y}$		0.26	0.26		$u_{c,rel}$
$X_{\scriptscriptstyle X}$ and $X_{\scriptscriptstyle Y}$	$\rm zm/(s^2 count)$	0.44	0.37	0.56	$u_{c,rel}$
Contributing Uncertainties					
Deform. model.			_	0.30	$u_{rel,\mathrm{Type}\mathrm{B}}$
Inc. angle, $\cos \theta$		0.03	0.03	0.16	$u_{rel,\mathrm{Type}\mathrm{B}}$
ETM mass, $M$	kg	0.01	0.01	0.05	$u_{rel,\mathrm{Type}\mathrm{B}}$
Sens. ETM rot.	m	0.41	0.31	0.09	$u_{rel,\mathrm{Type}\mathrm{B}}$
Opt. eff., $\eta_R$	W/W	0.03	0.10	0.40	$u_{rel,\mathrm{Type}\mathrm{B}}$
Rx resp., $\rho_{Rx}$	count/W	0.14	0.17	0.15	$u_{c,rel}$

by their amplitudes in spectra of the interferometer output signal, yields the Pcal X/Y calibration comparison factor,  $\chi_{XY}$ . Ideally,  $\chi_{XY} = 1$ . However, due to errors in factors that are not common to both end stations, e.g. the optical efficiency correction factors  $\eta_R$ , errors due to unintended rotation of the ETMs caused by Pcal beam positions offsets, or other calibration errors, it can deviate from unity. In May, 2023,  $\chi_{XY}$  was measured to be 1.0027.

The measured value of  $\chi_{XY}$  together with estimates of the uncertainties in contributions to displacement factors that are not common to both end stations allows us to calculate *combined* displacement factors,  $X_X^c$  and  $X_Y^c$ . These factors take into account the independent calibrations of both Rx sensors and the measured Pcal calibration ratio,  $\chi_{XY}$ . They are given by

$$X_X^c = X_X/C_X \text{ and } X_Y^c = X_YC_Y, \tag{5}$$

where  $C_X C_Y = \chi_{XY}$ . The correction factors are calculated using the weighted geometrical mean of 1 and  $\chi_{XY}$  [16]. For LHO at the start of the O4 observing run, with  $\chi_{XY} = 1.0027$ , they are  $C_X = 1.0012$  and  $C_Y = 1.0015$ . After applying the combined calibration correction factors in the front-end code, the Pcal X/Y combined calibration comparison factor,  $\chi_{XY}^c$ , now expected to be unity, is being calculated continuously during the observing run.

Figure 8 shows  $\chi_{XY}^c$  calculated during the O4 observing run. The analysis looks at periods of at least 10 hours duration when the interferometer is in the most sensitive observing-mode configuration. Contiguous, 1000-sec-long fast Fourier transforms (FFTs) are used to calculate the calibration comparison factors. The top panel shows the FFT

results from a typical observing-mode segment with a relative standard uncertainty of 0.01%. The mean values of  $\chi_{XY}^c$  measured each 1000 s during observing segments are plotted in the bottom panel with error bars given by the standard uncertainties. For the first two months the calibration ratio is close to 1.0000, as expected; it dips to about 0.999 between August and November. The cause of this drift is currently under investigation along with variations observed in other Pcal signals during the O4 run (see, for example, figure 7).

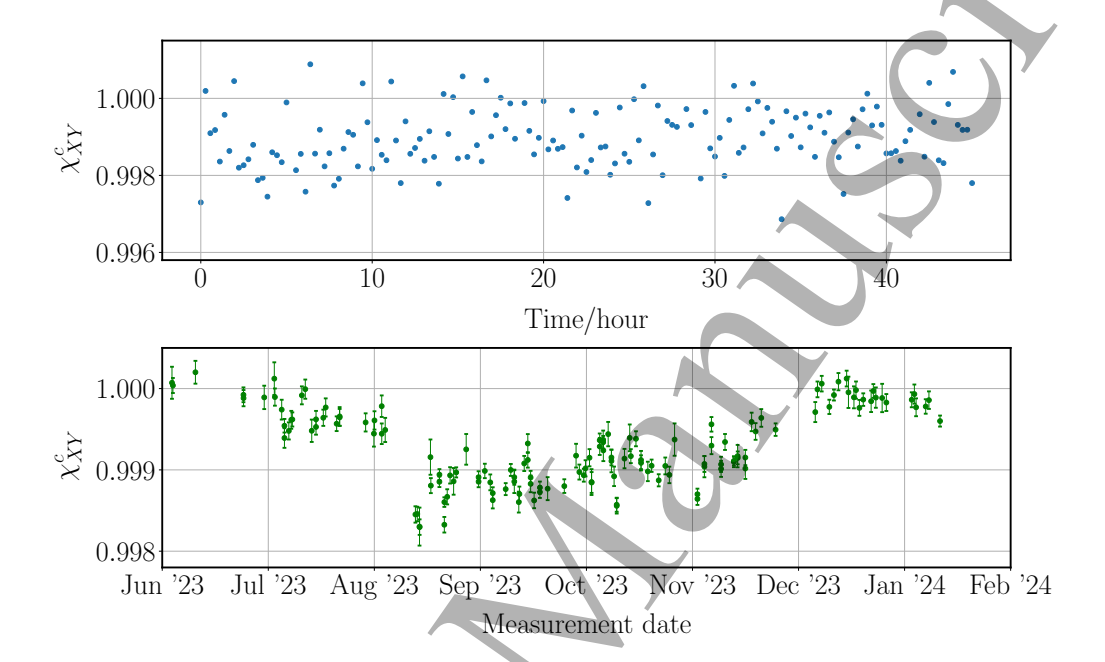
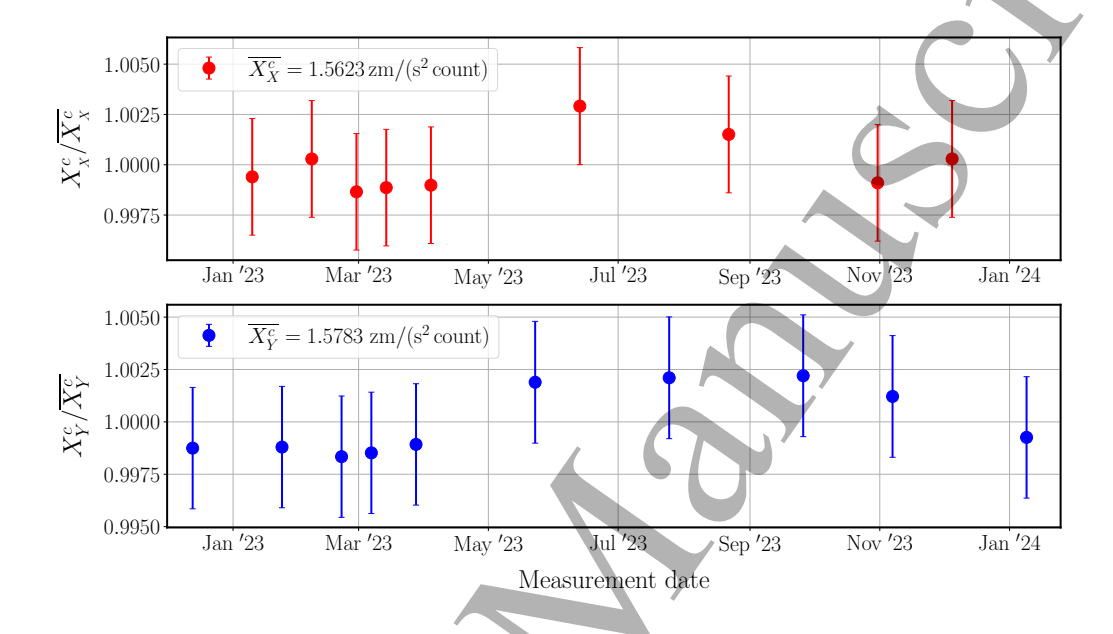


Figure 8. Calculated values of  $\chi_{XY}^c$  in (zm/count)/(zm/count) for the LHO detector during the O4 observing run. Top: Typical 1000-sec-long, contiguous FFT results during a 45-hour observation interval. Bottom: Mean  $\chi_{XY}^c$  values during observation intervals for the first eight months of the O4 observing run. The error bars are the relative standard uncertainties during the segments that vary in duration from 10 to 73 hours.

Measuring  $\chi_{XY}$  also enables reducing the uncertainties in the induced fiducial displacements that are due to factors that are not common to both ends. The largest factors at LHO are those due to unintended rotation of the ETM. These uncertainties are proportional to the dot product of the Pcal and interferometer beam offset vectors in (2). The LIGO Pcal beams are carefully positioned when the vacuum envelope is vented using targets that are bolted to the suspension structures surrounding the ETMs and their positions at the entrance apertures of the Rx sensors are monitored during operation. Thus the magnitude of their position offset vector is estimated to be less than 2 mm. However, though by design the interferometer beam should be centered on the ETM surface within a few millimeters, point absorbers in the ETM coating [41] have required operating the interferometer with beam offsets as large as 29 mm, increasing the uncertainty due to rotation by a factor of  $\sim 10$  over what was expected. The Virgo

Pcal beam is positioned at the center of the ETM surface within 10 mm relying on the mechanical positions of the input and output vacuum windows and the location of the ETM with respect to the vacuum envelope. The interferometer beam is centered on the ETM to within 1 mm, so the uncertainty due to unintended rotation is smaller than for LHO.

The uncertainties in  $C_X$  and  $C_Y$  listed in table 3 are given by the weighted relative standard uncertainty on the geometric mean of 1 and  $\chi_{XY}$ . It is significantly smaller than



**Figure 9.** Calculated combined displacement factors in zm/(s<sup>2</sup>count):  $X_X^c$  (*Top*) and  $X_Y^c$  (*Bottom*), for the LHO Pcal systems based on measurements performed between Dec. 2022 and Jan. 2024. The data are normalized to the mean of all the measurements, shown in the legends.

the quadrature sums of the relative uncertainties in the parameters contributing to  $X_X$  and  $X_Y$  that are not common to both end stations. The relative standard uncertainty in the combined displacement factors is calculated by summing in quadrature the relative uncertainty in  $C_X$  and  $C_Y$  with the uncertainties in the parameters that are common to both end stations (see table 2). For LHO during O4 the relative standard uncertainties in  $X_X^c$  and  $X_Y^c$  are 0.29%. Based on end stations measurements performed between Dec. 2022 and Jan. 2024, calculated Pcal combined displacement factors for the LHO Rx sensor output signals are plotted in figure 9. The error bars are the relative combined standard uncertainty of 0.29%.

The Pcal X/Y calibration comparison has not yet been implemented in Virgo. The uncertainties in the fiducial displacement calibration estimates given in table 3, at the level of 0.40%, are not combined to reduce the effect of the non-common uncertainties in the calibrations of the Pcal systems at the two end stations.

### 6. Conclusions

We have described a new scheme for calibrating the global network of gravitational wave observatories that involves laser power calibration transfer standards calibrated at both NIST and PTB. It is being implemented during the ongoing O4 observing run by the LIGO and Virgo projects, with the KAGRA project expected to join in 2024 and the LAO observatory to join later. A new NIST-PTB bilateral comparison using two upgraded transfer standards dedicated to this calibration scheme was carried out before the O4 observing run began in May 2023. The uncertainty in the DoE, 0.32% (k=2), was a factor of 2.5 smaller than for the previous NIST-PTB bilateral comparison, mostly attributed to NIST implementing a new primary standard with significantly lower calibration uncertainty.

We have described how the calibrations of the transfer standards used in the global calibration scheme were propagated to Pcal power sensors operating at observatory end stations and used to calibrate the Pcal-induced displacement fiducials. We have also described the calibration of the Pcal-induced displacement fiducials for the O4 observing run with estimated relative combined standard uncertainties of  $0.29\,\%$  at LHO and  $0.40\,\%$  at Virgo.

Currently at LHO, the Pcal-induced unintended rotation of the ETM that is sensed as longitudinal displacement by the interferometer is the dominant source of uncertainty. The impact of rotation is increased due to point absorbers in the ETM coatings that necessitate operating with interferometer beams displaced from the center of the optics by as much as 29 mm. A significant reduction in the impact of this source of uncertainty was realized by correcting for the measured ratio the Pcal calibrations at the two interferometer end stations, the Pcal X/Y calibration comparison factor. The end station mirrors at LLO have been replaced with optics with improved coatings that have less point defects, allowing operation with the interferometer beams located much closer to the center of the optics. This significantly reduces the impact of unintended Pcal-induced rotation. Replacement of the LHO ETMs is planned for after the O4 observing run.

At Virgo, the main sources of uncertainty come from the deformation modeling required by the use of a single-beam Pcal configuration and from uncertainties in the optical efficiency. These contributions will be reduced in future upgrades of the systems which are planned for after the O4 observing run. The setup will be switched to a two-beam configuration, incident through the rear anti-reflection coated surface of the ETM. The systems will be capable of switching to a one-beam configuration to maintain the ability to generate larger sensed displacements at high frequencies by exciting the internal vibrational modes of the ETM. The optical design and choice of vacuum windows will reduce optical losses and associated uncertainties.

Due to KAGRA being constructed much later than LIGO and Virgo, the Pcal systems are still being commissioned. Improvements are being made as issues are addressed. Efforts to realize more reliable calibration and reduce uncertainty have

focused on revising calibration procedures for the Pcal power sensors and developing methods to better estimate beam positions on the ETM surface [36]. The angles and positions of the beams incident on the power sensors, which use a different integrating sphere design than the other observatories, are expected to be the primary sources of uncertainty [42].

During the last observing run and in the interferometer's most sensitive frequency band near 150 Hz, at LIGO the estimated standard uncertainty in the calibration of the interferometer output signals was approximately 2 % [21]. Currently, this does not limit the extraction of intrinsic source parameters from detected GW signals [43]. However, as the number and signal-to-noise ratios of detected signals increase, lower interferometer calibration uncertainty will be required [13]. Eventually, relative calibration errors between observatories in the GW network could also limit GW science. The global Pcal calibration scheme and the methods for propagating NIST and PTB power sensor calibrations to the end station Pcal power sensors being developed and described here are intended to ensure that the uncertainty in the displacement fiducials used to calibrate the interferometer signals is not the limiting factor.

Other methods for assessing interferometer calibrations are being developed within the GW community. Because Einstein's theory of general relativity predicts the waveforms of coalescing binary systems of compact objects such as black holes or neutron stars, comparison of detected GW signals with predicted waveform can eventually provide astrophysical calibration [44, 45]. A method developed for investigating relative calibration errors between observatories in the network using coalescing binary black hole GW signals was implemented during the O3 observing run that ended in April 2020 [46]. The LHO and LLO detector calibrations agreed within 3.5% and those of the Virgo and LLO detectors agreed within 10%. With improved sensitivities and more detected events [47] this method should provide an accurate and independent assessment of the global relative calibration being implemented as described in this paper.

There is another significant ongoing effort within the GW community to implement a method that has been discussed for a long time that is analogous to Pcals for providing absolute displacement calibration [48, 49]. It involves installing rotating mass quadrupoles, referred to as *Newtonian* (NCal) or *Gravity* (Gcal) calibrators, outside the vacuum envelopes near the ETMs at the observatory end stations [50, 51, 52] These devices modulate the ETM position via variations of the Newtonian gravitational field as they rotate at rates as high as 100 Hz.

A system of multiple NCal actuators designed to reach sub-percent accuracy and precision [50, 53] was installed and commissioned at the Virgo observatory in preparation for the O4 observing run. Comparing the fiducial displacements of an ETM induced by both Pcal and NCal systems could help to identify systematic errors in these systems and thus reduce overall displacement calibration uncertainty. Long-term comparisons should also enable precise monitoring of the stability of the two calibration methods and thus pave the way for future upgrades of hardware and methods.

### Acknowledgements

This material is based upon work supported by NSF's LIGO Laboratory, which is a major facility fully funded by the National Science Foundation (NSF), and by the Virgo Collaboration and the European Gravitational Observatory, which are mainly funded by the French Centre National de la Recherche Scientifique (CNRS), the Italian Istituto Nazionale di Fisica Nucleare (INFN) and the Netherlands Organization for Scientific Research (NWO), and the KAGRA Collaboration. The authors are grateful for computational resources provided by the LIGO Laboratory and supported by NSF grants PHY-0757058 and PHY-0823459.

RB, DC, and SH acknowledge support from JSPS KAKENHI grant JP22H00135. DB, SK, and FL acknowledge the LSC Fellows program for supporting their research at LHO under NSF award PHY-1912598. DB acknowledges support from NSF awards OAC-2103662, PHY-2011334, and PHY-2308693. CG acknowledges support from the French Agence Nationale de la Recherche for the project ACALCO (ANR-21-CE31-0024).

Enlightening discussions with T. Tomaru and the work of J. Lewis and E. Makelele on evaluating and monitoring the LHO Pcal X/Y calibration comparison are gratefully acknowledged. The support of S. Assis de Souza Melo during Virgo Pcal installation and calibration is also gratefully acknowledged.

This paper carries LIGO document number LIGO-P2300412 and Virgo document number VIR-1071A-23.

### Data availability statement

The data that support the findings of this study are available upon request from the authors.

### References

- [1] Abbott B P et al (LIGO Scientific Collaboration and VIRGO Collaboration) 2016 Observation of gravitational waves from a binary black hole merger Phys. Rev. Lett. 116 061102
- [2] Abbott R, Abbott T D, Acernese F et al (The LIGO Scientific Collaboration and the Virgo Collaboration and the KAGRA Collaboration) 2021 GWTC-3: Compact binary coalescences observed by ligo and virgo during the second part of the third observing run arXiv (Preprint arXiv:2111.03606)
- [3] Abbott B P, Abbott R, Abbot T D et al (LIGO Scientific, Virgo) 2019 Properties of the binary neutron star merger GW170817 Phys. Rev. X 9 011001
- [4] Abbott B P, Abbott R, Abbot T D et al (The LIGO Scientific Collaboration and the Virgo Collaboration) 2018 GW170817: Measurements of Neutron Star Radii and Equation of State Phys. Rev. Lett. 121(16) 161101
- [5] Abbott B P, Abbott R, Abbot T D et al (Virgo, LIGO Scientific) 2017 On the Progenitor of Binary Neutron Star Merger GW170817 Astrophys. J. Lett. 850 L40
- [6] Abbott B P, Abbott R, Abbot T D et al (Virgo, LIGO Scientific) 2017 Estimating the Contribution of Dynamical Ejecta in the Kilonova Associated with GW170817 Astrophys. J. Lett. 850 L39
- [7] Albert A, Andre M, Anghinolfi M et al (Virgo, IceCube, Pierre Auger, ANTARES, LIGO Scientific) 2017 Search for High-energy Neutrinos from Binary Neutron Star Merger GW170817 with ANTARES, IceCube, and the Pierre Auger Observatory Astrophys. J. Lett. 850 L35
- [8] Roulet J and Zaldarriaga M 2019 Constraints on binary black hole populations from LIGO–Virgo detections Monthly Notices of the Royal Astronomical Society 484(3) 4216–4229
- [9] Abbott B P et~al (LIGO Scientific Collaboration and Virgo Collaboration) 2021 A gravitational-wave measurement of the Hubble constant following the second observing run of Advanced LIGO-Virgo ApJ 909 218
- [10] Chen H Y, Fishbach M and Holz D E 2018 A two percent Hubble constant measurement from standard sirens within five years *Nature* **562** 545–547
- [11] LIGO, Virgo, 1M2H, DES et al 2017 A gravitational-wave standard siren measurement of the hubble constant Nature 551 85
- [12] Lindblom L 2009 Optimal calibration accuracy for gravitational-wave detectors  $Phys.\ Rev.\ D$  80 042005
- [13] Vitale S, Del Pozzo W, Li T G F et al 2012 Effect of calibration errors on bayesian parameter estimation for gravitational wave signals from inspiral binary systems in the advanced detectors era Phys. Rev. D 85(6) 064034
- [14] Clubley D, Newton G, Skeldon K and Hough J 2001 Calibration of the Glasgow 10 m prototype laser interferometric gravitational wave detector using photon pressure *Phys. Lett. A* **283**
- [15] Karki S, Tuyenbayev D, Kandhasamy S et al 2016 The Advanced LIGO photon calibrators Rev. Sci. Instrum. 87 114503
- [16] Bhattacharjee D, Lecoeuche Y, Karki S et al 2020 Fiducial displacements with improved accuracy for the global network of gravitational wave detectors Class. Quantum Grav. 38 015009
- [17] Aasi J et al (LIGO Scientific Collaboration) 2015 Advanced LIGO Class. Quantum Grav. 32 074001
- [18] Acernese F et al (Virgo Collaboration) 2015 Advanced Virgo: a second-generation interferometric gravitational wave detector Class. Quantum Grav. 32 024001
- [19] Acernese F et al (Virgo Collaboration) 2019 Advanced Virgo Plus Phase I Design Report Virgo technical report URL https://tds.virgo-gw.eu/ql/?c=14430
- [20] Akutsu T et al (KAGRA Collaboration) 2019 KAGRA: 2.5 generation interferometric gravitational wave detector Nat. Astron. 3 35–40
- [21] Sun L, Goetz E, Kissel J S et al 2020 Characterization of systematic error in Advanced LIGO calibration Class. Quantum Grav. 37 225008
- [22] Acernese F et al (Virgo Collaboration) 2021 Calibration of Advanced Virgo and reconstruction of

- the detector strain h(t) during the observing run O3 Class. Quantum Grav. 045006
- [23] Akutsu T, Ando M, Arai K et al 2021 Overview of KAGRA: Calibration, detector characterization, physical environmental monitors, and the geophysics interferometer *Prog. Theor. Exp. Phys* **2021** ISSN 2050-3911
- [24] Goetz E, Kalmus P, Erickson S et al 2009 Precise calibration of LIGO test mass actuators using photon radiation pressure Class. Quantum Grav. 26 245011
- [25] Acernese F et al (Virgo Collaboration) 2018 Calibration of Advanced Virgo and Reconstruction of the Gravitational Wave Signal h(t) during the Observing Run O2 Class. Quantum Grav. 35 205004
- [26] Inoue Y, Hsieh B, Chen K et al 2023 Development of Advanced Photon Calibrator for KAGRA Rev. Sci. Instrum. 94 074502
- [27] Estevez D, Lagabbe P, Masserot A et al 2021 The Advanced Virgo photon calibrators Class. Quantum Grav. 38 075007
- [28] Spidell M, Lehman J, López M et al 2021 A bilateral comparison of NIST and PTB laser power standards for scale realization confidence by gravitational wave observatories Metrologia 58 055011
- [29] CCPR 2019 Guidelines for CCPR Key Comparison Report Preparation BIPM CCPR-G2 Rev.4
- [30] Karki S, Bhattacharjee D and Savage R L 2022 Toward calibration of the global network of gravitational wave detectors with sub-percent absolute and relative accuracy *Galaxies* **10** 42
- [31] Vaskuri A, Stephens M S, Tomlin N A et al 2021 High-accuracy room temperature planar absolute radiometer based on vertically aligned carbon nanotubes Opt. Express 29 22533
- [32] Stock K, Kück S and Brandt F 2003 Laserradiometrie PTB-Mitteilungen 113 361
- [33] Martin J E, Fox N P and Key P J 1985 A cryogenic radiometer for absolute radiometric measurements *Metrologia* **21**(3) 147
- [34] Werner L, Fischer J, Johannsen U and J H 2000 Accurate determination of the spectral responsivity of silicon trap detectors between 238 nm and 1015 nm using a laser-based cryogenic radiometer *Metrologia* 37 279
- [35] Hild S, Brikmann M, Danzmann K et al 2007 Photon pressure induced test mass deformation in gravitational-wave detectors Class. Quantum Grav. 24 5681–5688
- [36] Chen D  $et\ al\ ({\rm KAGRA\ collaboration})\ 2023\ {\rm Calibration\ of\ the\ gravitational\ wave\ telescope\ KAGRA\ PoS\ 444$
- [37] Bork R, Hanks J, Barker D et al 2020 An overview of the LIGO control and data acquisition system SoftwareX submitted (Preprint arXiv:physics/0111077)
- [38] Lagabbe P 2023 Improving the Advanced Virgo+ calibration with the photon calibrator for the O4 run PhD diss. Université Savoie Mont Blanc URL https://theses.hal.science/tel-04280527v1
- [39] Taylor B N and Kuyatt C E (U.S. Department of Commerce, Washington, D.C.) 1994 Guidelines for evaluating and expressing the uncertainty of NIST measurement results NIST Technical Note 1297 URL https://www.nist.gov/pml/nist-technical-note-1297
- [40] Yamamoto H and Vajente G 2020 Private communication LIGO
- [41] Brooks A F, Yamamoto H, Vajente G et al 2020 Point absorbers in Advanced LIGO Applied Optics 60 4047
- [42] Fujii S  $et\ al\ ({\rm KAGRA\ collaboration})\ 2023\ {\rm Calibration\ of\ the\ integrating\ sphere\ for\ O4\ in\ KAGRA\ gravitational\ wave\ telescope\ PoS\ 444$
- [43] Payne E, Talbot C, Lasky P et al 2020 Gravitational-wave astronomy with a physical calibration model Phys. Rev. D 102 122004
- [44] Essick R and Holz D 2019 Calibrating gravitational-wave detectors with GW170817 Class. Quantum Grav. 36 125002
- [45] Pitkin M, Messenger C and Wright L 2019 Astrophysical calibration of gravitational-wave detectors. *Phys. Rev.* **D93** 1062002
- [46] Alléné C, Andres N, Assiduo M et al 2011 Relative calibration of the LIGO and Virgo detectors

using astrophysical events from their third observing run Class. Quantum Grav. 39 195019

- [47] Abbott B P et al (LIGO Scientific, VIRGO and KAGRA Collaborations) 2018 Prospects for observing and localizing gravitational-wave transients with advanced LIGO, Advanced Virgo and KAGRA Living Rev. Relativ. 21 3
- [48] Mio N, Tsubono K and Hirakawa H 1987 Experimental test of the law of gravitation at small distances *Phys. Rev. D* **36** 2321
- [49] Matone L, Raffai P, Márka S et al 2007 Benefits of artificially generated gravity gradients for interferometeric gravitational-wave detectors Class. Quantum Grav. 24 2217
- [50] Estevez D, Lieunard B, Marion F et al 2018 First tests of a Newtonian calibrator on an interferometric gravitational wave detector Class. Quantum Grav. 35 235009
- [51] Inoue Y, Haino S, Kanda N et al 2018 Improving the absolute accuracy of the gravitational wave detectors by combining the photon pressure and gravity field calibrators *Phys. Rev. D* **98**(2) 022005
- [52] Ross M P, Mistry T, Datrier L et al 2021 Initial results from the LIGO Newtonian calibrator Phys. Rev. D 104 082006
- [53] Estevez D, Mours B and Pradier T 2021 Newtonian calibrator tests during the Virgo O3 data taking Class. Quantum Grav. 38 075012